Kinetics and mechanism of the electrochemical reduction of molecular oxygen on platinum in KOH: influence of preferred crystallographic orientation

C. F. ZINOLA, A. M. CASTRO LUNA, W. E. TRIACA, A. J. ARVIA

Instituto de Investigaciones Fisicoquímicas Teóricas y Aplicadas (INIFTA), Universidad Nacional de La Plata, Sucursal 4, Casilla de Correo 16, (1990) La Plata, Argentina

The oxygen electroreduction reaction has been studied at both preferred oriented and conventional polycrystalline platinum rotating disc electrodes in x M KOH $(0.05 \leq x \leq 3.0)$ aqueous solutions under oxygen saturation at 25° C. At low current densities, Tafel lines with slope -0.060 V decade^{-1} have been obtained at all platinum electrodes. At high current densities, higher Tafel slopes ranging from -0.18 to -0.40 V decade^{-1} have been observed, depending on the type of preferred oriented Pt and KOH concentration. Rotating ring-disc electrode data have shown that a higher amount of H_2O_2 is produced on one type of preferred oriented surface at all KOH concentrations. A complex reaction scheme has been used to evaluate the electrochemical rate constants of the reaction steps at three platinum electrodes.

1. Introduction

The oxygen electroreduction reaction (OERR), perhaps the electrochemical reaction most frequently found in various areas of different scientific interest [1, 2], has been thoroughly investigated at platinum electrodes in aqueous solutions [3]. Steady state kinetic data of OERR in aqueous alkaline solution obey different Tafel relationships depending on whether the low current density (l.c.d.) or high current density (h.c.d.) ranges are considered. In the l.c.d. region the Tafel slope is $b_T = -0.06$ V decade^{-1}, whereas at h.c.d., values of b_T comprised between -0.12 to -0.30 V decade^{-1} at 25° C have been obtained [4–7].

The OERR kinetics on platinum in aqueous solutions has been explained by a mechanism involving two parallel paths: the first path consists of a four-electron transfer direct reduction of oxygen to OH$^-$ ion, and the second path involves a two-electron transfer process leading from oxygen to H_2O_2, which can be further reduced to OH$^-$ ion in a following stage. The relative contribution of each path to the overall reaction varies with the experimental conditions [4]. The OERR mechanism, however, appears to be more complicated, at least in acid, as it becomes sensitive to the distribution and dominating type of crystallographic faces on polycrystalline facetted platinum, as well as on platinum single crystals [8, 9].

The formation of H_2O_2 in alkaline media [5, 6], in aqueous 1 M H_2SO_4 [9] and in concentrated H_3PO_4 [10] solutions in the course of the OERR, has already been reported. The H_2O_2 electroformation reaction itself is influenced by both platinum crystallographic orientation and anion surface blockage [9]. The

influence of surface blockage on the OERR in alkaline solutions deserves further work as a deeper understanding of this effect may offer a more comprehensive explanation of the OERR mechanism over the entire pH range from acid to alkaline solutions. This work pays special attention to the role played by H_2O_2 formation in the kinetics of the OERR at different preferred oriented polycrystalline platinum electrodes in alkaline solution, based on data resulting from rotating disc and ring-disc electrode techniques.

2. Experimental details

The OERR was studied at polycrystalline platinum (spectroscopic quality) rotating disc (3 mm dia.) working electrodes which were preferentially oriented to produce two distinguishable types of surface topographies (A and B). These surfaces were facetted in well-defined directions. The technique for preparing electrodes A and B has been described elsewhere [11].

A large platinized-Pt plate (10 cm^2 geometric area) counter electrode close to the working electrode, for minimizing ohmic drop, was employed. A reversible hydrogen electrode (RHE) in the solution, which was connected to the rest of the cell through a Luggin–Haber capillary tip, was used as reference electrode. Except when otherwise noted, all potentials in the text were referred to RHE.

A Tacussel rotating ring-disc electrode (RRDE) device was also used; N, the experimental collection efficiency of this device, was 0.22 [12].

Prior to the preparation of the surfaces, the polycrystalline Pt discs were mechanically polished with different grades of alumina down to 0.05 μm grit,

repeatedly rinsed with triply-distilled water, and finally, immersed in 0.5 M H_2SO_4 for 1 h. The working electrode real surface area was estimated by comparing the H-adatom voltammetric charge recorded at $0.1 \, V \, s^{-1}$ to the H-atom monolayer charge density on the different platinum surfaces [13].

Aqueous xM KOH solutions $(0.05 \leqslant x \leqslant 3.0)$ were prepared from KOH (Merck p.a.) and Millipore*-Milli-Q* water. Runs were made at 25° C under either nitrogen or oxygen (99.99% purity) atmosphere.

RRDE data were run in the $500 \leqslant \omega \leqslant 2000$ r.p.m. range, although most of the RDE data has been obtained at 2000 r.p.m. In these cases, E_D, the disc electrode potential, was scanned at $0.01 \, V \, s^{-1}$ from 1.2 to 0.05 V, while E_R, the ring electrode potential, was held at 1.2 V. At this potential the H_2O_2 produced on the disc could be electrooxidized on the ring under limiting current conditions.

Steady state potentiostatic polarization curves were obtained at $\omega = 2000$ r.p.m. To assure a reproducible initial surface the working electrode was held 5 s at 1.40 V, a potential at which a full coverage of platinum surface by O-containing species was attained, followed by an electroreduction step at 0.05 V for 5 s. At each potential, the stationary OERR current was obtained after 5 min potential holding. This time was sufficient to reach a current value with less than 0.5% of variation.

3. Results

3.1. Cyclovoltammetric response of different platinum electrodes

The cyclovoltammograms obtained with the different platinum electrodes in aqueous 1.0 M KOH in the H-adatom potential range at $0.1 \, V \, s^{-1}$ are shown in Fig. 1 together with those obtained in aqueous 0.5 M H_2SO_4. The cyclovoltammograms in 0.5 M H_2SO_4 can be used as fingerprints of the platinum electrode surfaces [11].

Cyclovoltammograms in 1.0 M KOH show the typical H-adatom electrosorption potential region from 0.05 to about 0.50 V, the O-adatom electrosorption and incipient oxide formation region from 0.60 to 1.50 V, and the so-called double layer region in between. The H-adatom electrosorption voltammograms present a multiplicity of current peaks associated with different H-adatom bonding energies at platinum surface sites. In alkaline solutions, the height of strongly adsorbed H-adatom current peaks is always significantly lower than that of those peaks found in acidic media. Besides, the double layer potential window in alkaline media becomes narrower than in acidic solutions.

The shape of voltammograms obtained on A-type Pt depend on whether 0.5 M H_2SO_4 or 1.0 M KOH has been used (Fig. 1). In acid, the voltammetric features resemble those already reported for stepped Pt(1 0 0) surfaces in the same solution. They are
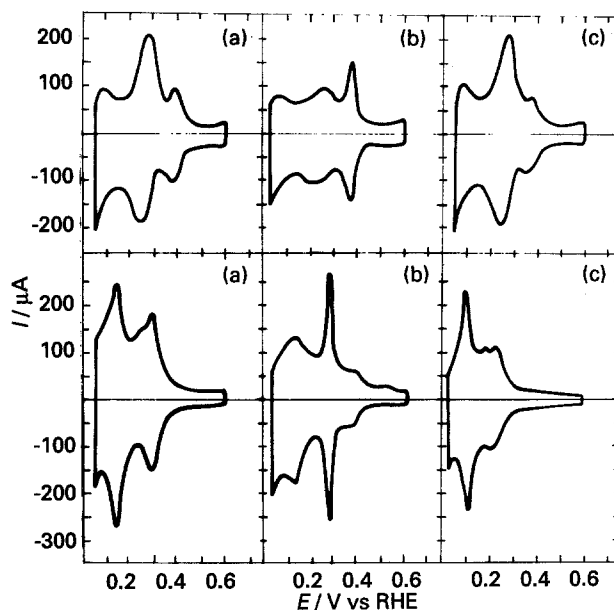

Fig. 1. Cyclovoltammograms run at $0.1 \, V \, s^{-1}$ in 1 M KOH (upper curve) and 0.5 M H_2SO_4 (lower curve) at 25° C. (a) Polycrystalline Pt, (b) A-type Pt, (c) B-type Pt.

characterized by a high contribution of strongly adsorbed H-adatoms, and a small contribution of weakly adsorbed ones. The multiplicity of conjugated peaks at about 0.40 V, which appears in 0.5 M H_2SO_4, is not observed in 1.0 M KOH solutions. Strongly adsorbed H-adatom peaks are displaced to 0.38 V in 1.0 M KOH, although the separation between strongly and weakly adsorbed H-adatom peaks remains about 0.12 V in both solutions [14, 15].

Voltammograms run on B-type Pt electrodes in 0.5 M H_2SO_4 show a relatively large contribution of weakly adsorbed H-adatoms, as a pair of reversible conjugated peaks at 0.10 V. Likewise, another relatively smaller contribution appears as a pair of conjugated peaks at about 0.32 V. The features of these voltammograms resemble those of a stepped reconstructed Pt(1 1 1) surface electrode. The cyclovoltammograms of B-type platinum electrodes in 1.0 M KOH are rather similar to those resulting from untreated polycrystalline platinum electrodes, except that at B-type platinum a minor contribution of strongly adsorbed H-adatom peaks can be observed [14, 15].

3.2. Rotating disc data

Typical OERR disc current (I_D) against disc potential (E_D) plots obtained at different platinum working electrodes at 500, 1000, 1500 and 2000 r.p.m. in 0.1 M KOH, are shown in Fig. 2. The initial nonzero part of these plots, covering the 0.95–0.80 V range, becomes independent of the rotation speed, ω. The range of the slowly increasing currents at higher overpotentials is broader as ω is increased, as expected for an electrochemical reaction under mixed control. At about 0.70 V mass transport kinetic contributions become significant and determine the appearance of a well-defined cathodic current plateau (I_{LD}) for
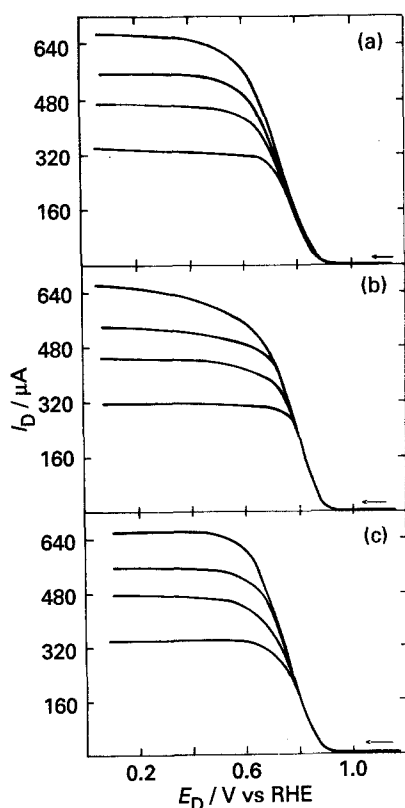
Fig. 2. I_D/E_D voltammograms recorded in oxygen-saturated 0.1 M KOH solution at $\omega = 500$, 1000, 1500, 2000 r.p.m. (Power to upper curves). Sweep rate $v = 0.01\ \text{V s}^{-1}$, $T = 25°$ C. (a) Polycrystalline Pt, (b) A-type Pt, (c) B-type Pt.
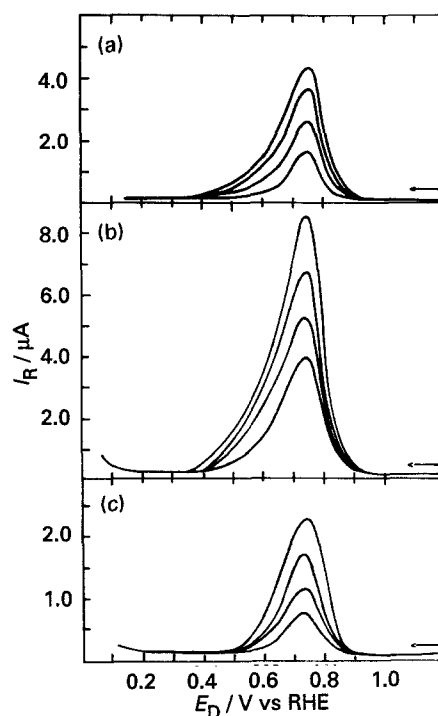

Fig. 3. I_R/E_D voltammograms recorded in oxygen-saturated 0.1 M KOH solution at $\omega = 500$, 1000, 1500 and 2000 r.p.m. (lower to upper curves). Sweep rate $v = 0.01\ \text{V s}^{-1}$, $T = 25°$ C. $E_R = 1.2$ V. (a) Polycrystalline Pt, (b) A-type Pt, (c) B-type Pt.

$E < 0.40$ V. The height of this plateau increases linearly with the square root of ω. Sometimes a slight hump at 0.20 V follows the appearance of the current plateau. This hump presumably results from the initial H-adatom adsorption on platinum.

The above description of polarization curves applies to higher KOH concentrations, the height of the OERR current plateau decreases as the KOH concentration is increased. Nevertheless, when the current is referred to unit oxygen concentration in the solution, calculated from oxygen solubility data [16, 17], KOH concentration independent current plateau values at each ω are found. The small variations of these figures can be attributed to the KOH concentration dependence on both the oxygen diffusion coefficient and the solution viscosity (Table 1) [16–19].

3.3. Rotating ring disc data

Rotating ring-disc measurements were used to distin-

guish between series and parallel mechanisms in the OERR at different platinum electrodes in KOH solutions.

Plots of disc (I_D) and ring (I_R) currents as a function of E_D at different ω (Figs 2 and 3) were obtained in 0.1 M KOH. In these runs, E_R was set to 1.20 V, a potential at which the H_2O_2 formed at the disc can be electrooxidized to oxygen at the ring under diffusion limiting conditions.

The value of I_R increases, due to H_2O_2 electrooxidation, with both ω and E_D, but I_R reaches a maximum value at $E_D = 0.73$ V, a potential which coincides with the inflection point at the I_D against E_D plot.

The fraction of the total reaction proceeding via the H_2O_2 path can be estimated from the following expression, considering $N = 0.22$ [20]:

$$F_{H_2O_2}(\%) = \frac{I_R/N}{I_R/N + I_D} \times 100 \tag{1}$$

At 2000 r.p.m. in 0.1 M KOH it results in A-type platinum electrode $F_{H_2O_2} = 12\%$, in B-type platinum $F_{H_2O_2} = 4\%$ and in polycrystalline platinum $F_{H_2O_2} = 6\%$. The value of F decreases abruptly at

Table 1. pH, KOH solution viscosity, oxygen solubility, oxygen diffusion coefficient, and OERR limiting current densities at $\omega = 2000$ r.p.m. at 25° C. j_L is the limiting current density referred to oxygen concentration

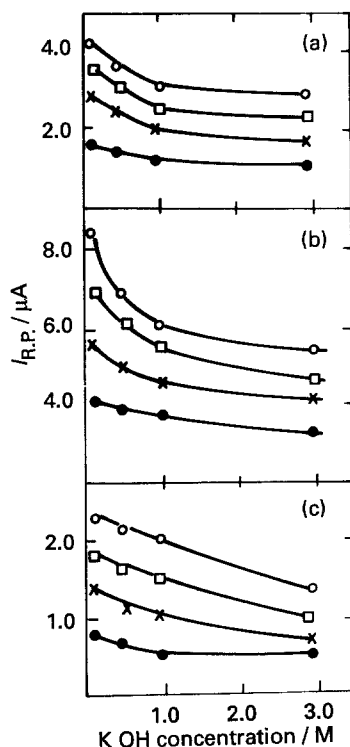| (KOH) /mol dm^{-3}	pH	η_{KOH} /cPs	S_{O_2} /mol cm^{-3} $\times 10^6$	D_{O_2} /cm^2 s^{-1} $\times 10^5$	j_{LD} /μA cm^{-2}	j_L /A cm mol^{-1}
0.05	12.6	1.005	1.235	1.95	3100	2510
0.10	12.9	1.013	1.210	1.87	2950	2480
0.50	13.5	1.064	1.031	1.68	2710	2570
1.0	13.8	1.128	0.843	1.43	2140	2540
3.0	14.0	1.350	0.377	1.00	910	2455

Fig. 4. Dependence of the ring peak current (I_{RP}) for H_2O_2 oxidation during OERR on the KOH concentration. $T = 25°$ C. (a) Polycrystalline Pt, (b) A-type Pt, (c) B-type Pt. (o) 500, (□) 1000, (×) 1500, and (•) 2000 r.p.m.

the highest KOH concentration on A-type platinum. The dependence of the peak current at the ring (I_{RP}) on KOH concentration at different ω (Fig. 4) shows a decrease in H_2O_2 generation at all Pt working electrodes as KOH concentration is increased.

4. Analysis of results

A qualitative analysis of OERR kinetic data on platinum electrodes in KOH solutions suggests that OERR is a complex electrocatalytic surface process in which adsorption and desorption of reactants, products and intermediates, as well as the influence of the platinum substrate structure, should be considered. Earlier work has described the four-electron global OERR through a reaction pathway involving at least two main parallel reaction paths which are linked by a common reaction intermediate.

From the mechanistic standpoint these results in alkaline solution are analysed within a framework which is essentially the same as that earlier used for results obtained in acid solutions.

4.1. *Polarization curves*

For a quantitative analysis of steady state kinetic data, mass transport correction at polarization curves was firstly considered. These curves were plotted as E_D (NHE) against $\log j$, where j is the electroreduction current density, defined as the current/real working electrode area ratio, and E_D is the electrode potential referred to NHE scale. They show, for all platinum electrodes, l.c.d. and h.c.d. linear regions in all KOH concentrations (Fig. 5) and the slopes of these lines are $(b_T)_{l.c.d.} = (\Delta E/\Delta \log j)_{l.c.d.} = -0.060$ V decade^{-1}, and $(b_T)_{h.c.d.} = (\Delta E/\Delta \log j)_{h.c.d.}$ ranging from -0.180 to -0.400 V decade^{-1} at 25° C. These two Tafel lines agree with previously reported results for dilute alkaline solutions at polycrystalline platinum electrodes [5–7].

The $(b_T)_{l.c.d.}$ slope range covers approximately two decades in j from the rest potential ($E_{rest} = 0.15$ V vs NHE in 0.1 M KOH) to 0.03 V, whereas the $(b_T)_{h.c.d.}$ slope range covers more than a decade in j from about 0.03 to -0.30 V in the NHE scale.

The extrapolation of Tafel lines to the oxygen electrode reversible potential ($E^0_{O_2/OH^-} = 0.467$ V vs NHE in 0.1 M KOH) has allowed estimation of the value of j_0, the OERR exchange current density from the two Tafel regions. Kinetic data resulting from diffusion-free conditions are assembled in Table 2. The values of $(b_T)_{h.c.d.}$ and $(j_0)_{h.c.d.}$ on polycrystalline platinum increase with KOH concentration, but these dependencies cannot be clearly found for A and B-type platinum electrodes. Values of j_0 were further corrected to account for the KOH concentration dependent oxygen solubility [16, 17]. These values are given as k_{O_2} in Table 2.

Kinetic data shown in Table 2 prove that the OERR rate is enhanced as the KOH concentration is increased up to 3 M. At KOH concentrations higher than 3 M, this behaviour is no longer observed, particularly in the h.c.d. region. This fact
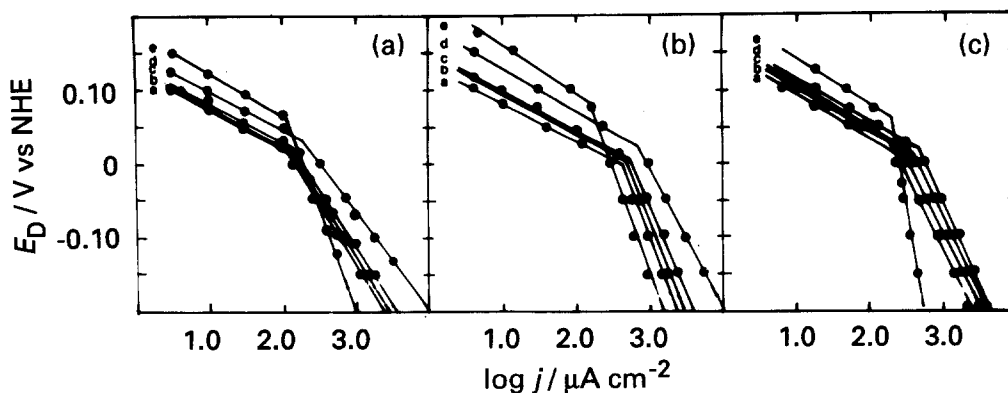

Fig. 5. Tafel lines for OERR in (a) polycrystalline Pt, (b) A-type Pt, (c) B-type Pt in oxygen-saturated KOH solutions. (a) 0.05, (b) 0.1, (c) 0.5, (d) 1 and (e) 3 M.

Table 2. Kinetic parameters for OERR in the l.c.d. and h.c.d. regions in KOH solutions at 25° C. k_{O_2} is the exchange current density referred to oxygen unity concentration

(KOH) /mol dm^{-3}	$b_{T_{l.c.d.}}$ /V dec^{-1}	$jo_{l.c.d.}$ /μA cm^{-2}	$b_{T_{h.c.d.}}$ /V dec^{-1}	$jo_{h.c.d.}$ /μA cm^{-2}	$k_{O_{l.c.d.}}$ /A cm mol^{-1}	$k_{O_{h.c.d.}}$ /A cm mol^{-1}
Polycrystalline platinum						
0.05	−0.055	3.2×10^{-7}	−0.180	0.1	3×10^{-7}	8×10^{-2}
0.10	−0.052	5.0×10^{-7}	−0.200	0.2	4×10^{-7}	2×10^{-1}
0.50	−0.065	6.3×10^{-7}	−0.215	0.6	6×10^{-7}	6×10^{-1}
1.0	−0.053	1.0×10^{-6}	−0.270	1.6	1×10^{-6}	2
3.0	−0.055	5.6×10^{-5}	−0.300	17.8	1×10^{-4}	47
A-type platinum						
0.05	−0.053	3.2×10^{-7}	−0.320	8.0	3×10^{-7}	6
0.10	−0.060	6.3×10^{-6}	−0.315	7.9	5×10^{-6}	7
0.50	−0.055	3.2×10^{-5}	−0.300	15.8	1×10^{-5}	15
1.0	−0.055	1.0×10^{-5}	−0.310	19.9	3×10^{-5}	24
3.0	−0.065	3.1×10^{-3}	−0.300	14.1	8×10^{-3}	38
B-type platinum						
0.05	−0.060	3.5×10^{-6}	−0.240	10.0	3×10^{-6}	8
0.10	−0.062	1.0×10^{-5}	−0.290	12.6	8×10^{-6}	10
0.50	−0.060	5.6×10^{-5}	−0.290	17.8	5×10^{-5}	17
1.0	−0.055	1.0×10^{-4}	−0.250	31.6	1×10^{-4}	38
3.0	−0.050	6.3×10^{-5}	−0.415	20.0	2×10^{-4}	53

may imply that above 3 M KOH, either a different OERR mechanism at h.c.d. operates, or the properties of the interface are modified, giving rise to different O_2–Pt surface initial interactions.

4.2. Reaction order with respect to oxygen

The OERR kinetics are often assumed to be first order with respect to the reactant in all reaction steps. To prove this condition the linearity of the $I_D^{-1/2}$ against
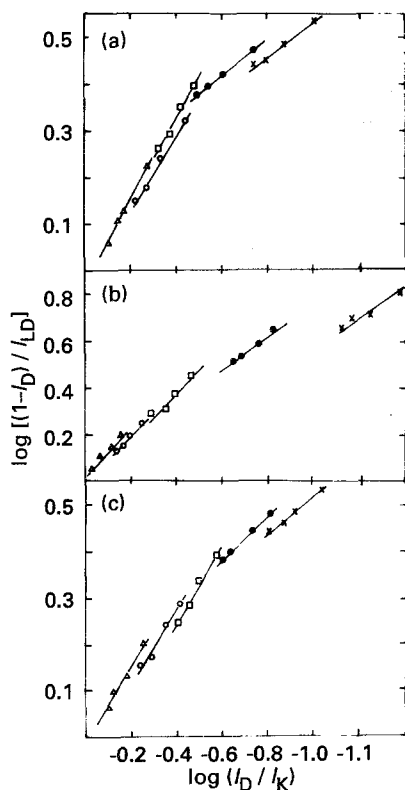

Fig. 6. $\log (1 - I_D/I_{LD})$ against $\log (I_D/I_k)$ plots. (a) Polycrystalline Pt, (b) A-type Pt, (c) B-type Pt. Oxygen-saturated 0.1 M KOH, $T = 25°$ C. (×) 0.52, (●) 0.62, (□) 0.70, (○) 0.75 and (△) 0.80 V.

$\omega^{-1/2}$ plot is established. For a first reaction order with respect to oxygen, $p = 1$, this plot arises from the Koutecky–Levich equation [21]

$$(1/I_D)^{1/p} = (1/I_k)^{1/p} + \frac{(I_D)^{1-1/p}}{B\omega^{1/2}} \qquad (2)$$

where $B = 0.62 n F c_{O_2}^0 D_{O_2}^{2/3} \nu^{-1/6} A_D$ is known as Levich slope, and I_k is the net OERR kinetic current.

A plot of $\log (I_D/I_k)$ against $\log (1 - I_D/I_{LD})$ is often handled to decide whether p is a potential dependent parameter. According to Equation 2, at constant ω, the slope of this linear plot should be p. These plots were made using data obtained at different potentials. Typical results are shown in Figs 6 and 7 for 0.1 M KOH. Values of $p = 1.0 \pm 0.2$ were found at potentials higher than 0.60 V for all platinum electrodes. A coincidence between the experimental slope, $B_{exp} = 0.052$ mA cm^2 r.p.m.$^{1/2}$ and Levich slope calculated with $c_{O_2}^0$, D_{O_2} and η given in Table 1 has been found. Otherwise, at potentials lower than 0.60 V the same data treatment leads to $p = 2.0 \pm 0.2$, a value which is worth noticing for the coincidence between the experimental ($B_{exp} = 0.057$ mA cm^2 r.p.m.$^{1/2}$) and Levich slope.

4.3. Influence of H_2O_2 and supporting electrolyte

Further OERR results were obtained in 0.1 M KOH in the presence of H_2O_2 at the μM concentration range on A and B-type platinum working electrode. In both cases, an increase in the value of $(b_T)_{h.c.d.}$ with H_2O_2 concentration was found. Correspondingly, in the Tafel region a gradual decrease in cathodic current at a constant E_D was observed. This effect becomes more remarkable as H_2O_2 concentration is increased. It should be noted that the same trend was found when a supporting electrolyte, such as 0.5 M K_2SO_4 instead of H_2O_2, was added to 0.1 M KOH.
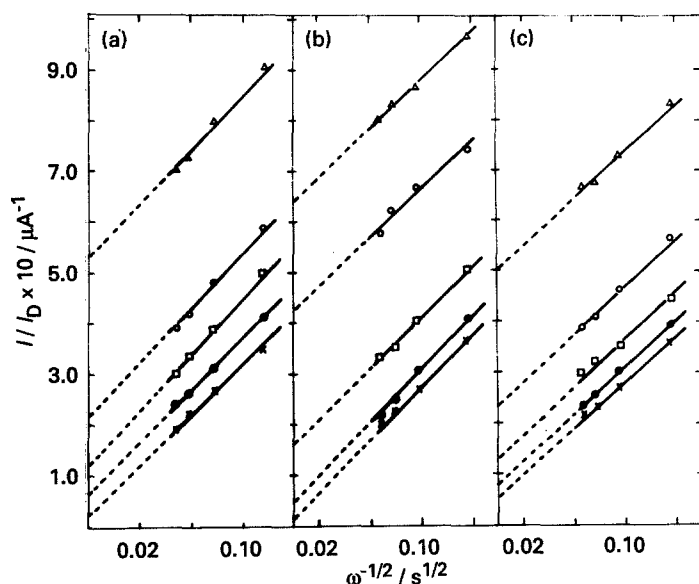
Fig. 7. I_D^{-1} against $\omega^{-1/2}$ plots. (a) Polycrystalline Pt, (b) A-type Pt, (c) B-type Pt. Oxygen-saturated 0.1 M KOH, $T = 25°$C. (×) 0.52, (●) 0.62, (□) 0.70, (○) 0.75 and (△) 0.80 V.

A value of $(b_T)_{h.c.d.}$ higher than $2.3(2RT/F)$ may be related to blockage of the working electrode surface by either reaction intermediates or reaction products such as H_2O_2, and by specific adsorption of SO_4^{2-} anions. These ions are adsorbed on platinum in 0.5 M $KF + 0.5$ M $HF + 0.01$ M K_2SO_4 in the 0.2–1.0 V range as proved by FTIRS investigations [22]. In alkaline solutions SO_4^{2-} ion adsorption on platinum implies a competitive process involving both SO_4^{2-} and OH^- ions, reaction intermediates, products and water itself. The relative contribution of each adsorbable species should depend considerably on the solution composition and applied potential, i.e. on their individual electrosorption isotherm [23].

5. Discussion

5.1. General considerations

The kinetics of the OERR at platinum in alkaline solutions involves a l.c.d. and a h.c.d. Tafel slope as given in Table 2. OERR kinetics in the l.c.d. range have been explained as a consecutive four-electron transfer pathway involving a single electron transfer step yielding adsorbed O-containing species under Temkin adsorption conditions as a rate determining step (r.d.s.) [6, 7]. Conversely, the OERR mechanism in the h.c.d. range is far from being well understood; it is usually given in terms of a chemical r.d.s. such as oxygen-adsorption onto the platinum surface. This general kinetic and mechanistic description applies qualitatively to the OERR at high concentration acidic media [10]. Thus, the polarization curves

obtained in purified 85.5% H_3PO_4 exhibit a l.c.d. Tafel line with a slope of $2.3(RT/F)$ and a h.c.d. Tafel slope $(b_T)_{h.c.d.} = -0.22$ V decade^{-1} at potentials lower than 0.9 V [10].

Srinivasan *et al.* [5] attributed the h.c.d. region Tafel slope on polycrystalline platinum in KOH solutions to oxygen diffusion towards the working electrode surface as a r.d.s. at high cathodic overpotentials. This explanation, which seems reasonable as a first approach, is insufficient to account for the results of this work which prove a definite influence of platinum surface morphology at high cathodic overpotentials.

Another interpretation advanced by Yeager *et al.* [24] took into account a r.d.s. related to the presence of a relatively high platinum surface coverage by adsorbed reactants or products. In principle, this explanation is consistent with those kinetic results obtained in 0.1 M KOH after the addition of either H_2O_2 or SO_4^{2-}, as referred to in Section 4.3.

The conclusions from preceding studies of OERR have been considered in several reaction schemes which were proposed involving either consecutive or parallel steps [25–31].

5.2. Likely reaction pathway

Among these reaction schemes, that proposed by Damjanovic *et al.* has been successfully applied to OERR kinetic data on platinum substrate in both acid and alkaline solutions. This reaction scheme can be presented as follows:
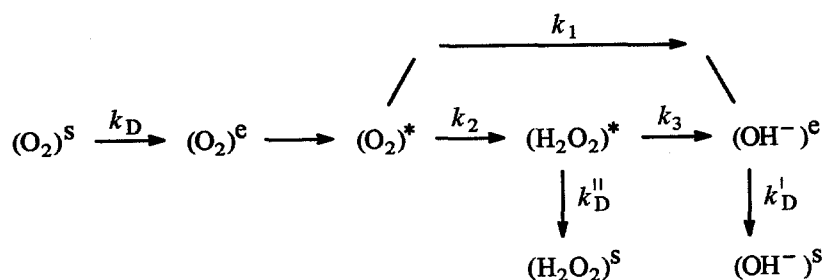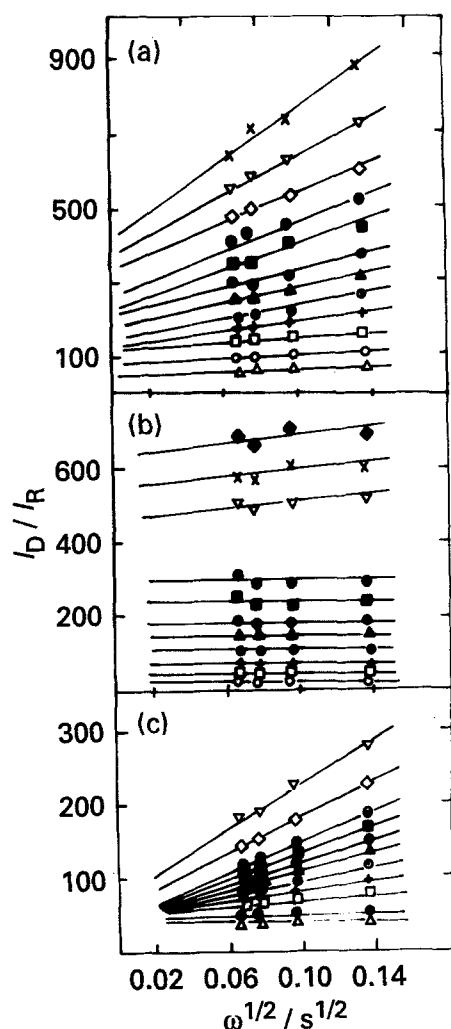
Fig. 8. I_D/I_R against $\omega^{-1/2}$ plots. (a) Polycrystalline Pt, (b) A-type Pt, (c) B-type Pt. Oxygen-saturated 0.1 M KOH solution. $T = 25°$ C. ($\blacklozenge$) 0.50, ($\times$) 0.52, ($\triangledown$) 0.54, ($\diamond$) 0.56, ($\oplus$) 0.58, ($\blacksquare$) 0.60, ($\ominus$) 0.62, ($\blacktriangle$) 0.64, ($\odot$) 0.66, (+) 0.68, ($\square$) 0.70, ($\bigcirc$) 0.75 and ($\triangle$) 0.80 V.
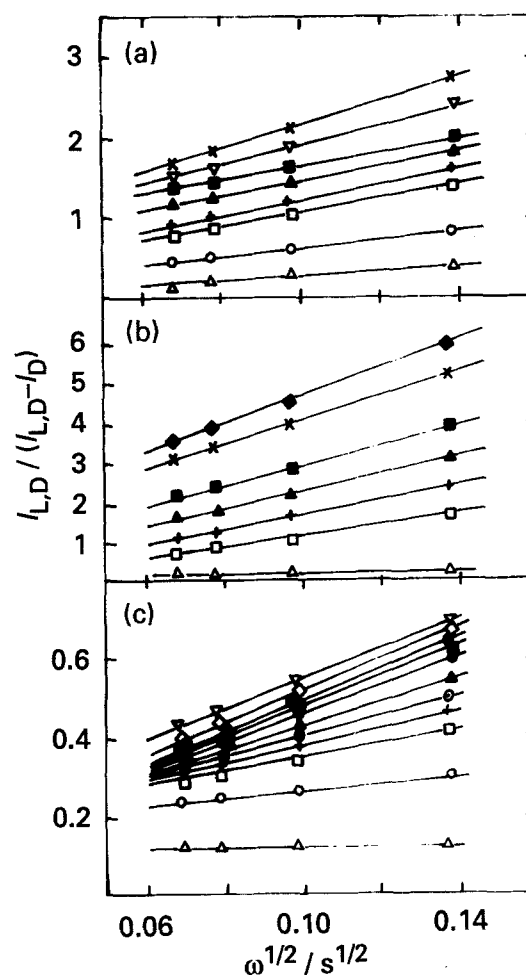
Fig. 9. $I_{L,D}/(I_{L,D} - I_D)$ against $\omega^{-1/2}$ plots. (a) Polycrystalline Pt, (b) A-type Pt, (c) B-type Pt. Oxygen-saturated 0.1 M KOH solution. $T = 25°$ C. ($\blacklozenge$) 0.50, ($\times$) 0.52, ($\triangledown$) 0.54, ($\diamond$) 0.56, ($\oplus$) 0.58, ($\blacksquare$) 0.60, ($\ominus$) 0.62, ($\blacktriangle$) 0.64, ($\odot$) 0.66, (+) 0.68, ($\square$) 0.70, ($\bigcirc$) 0.75 and ($\triangle$) 0.80 V.

where k_D, k_D' and k_D'' are the mass transport rate constants for oxygen molecules from the bulk of the solution towards the platinum working electrode surfaces, and the OH^- and H_2O_2 transport from the working electrode surface to the bulk solution, respectively, k_i is the electrochemical rate constant for the ith step, and the superscripts s, e and * denote the species in the bulk of the solution, at the interface, and adsorbed on platinum, respectively. The validity of this mechanism can be tested through RRDE data, as all the kinetic constants involved can be evaluated.

Scheme 3 predicts the following I_D/I_R ratio against $\omega^{-1/2}$, and the $I_{LD}/(I_{LD} - I_D)$ ratio against $\omega^{-1/2}$ relationships [4, 19, 30]:

$$\frac{I_D}{I_R} = \frac{1}{N}\left[1 + \frac{2k_1}{k_2} + \frac{2k_3(1 + k_1/k_2)}{0.62D_{O_2}^{2/3}\nu^{-1/6}}\omega^{-1/2}\right] \quad (4)$$

and

$$\frac{I_{LD}}{I_{LD} - I_D} = 1 + \frac{(k_1 + k_2)}{0.62D_{O_2}^{2/3}\nu^{-1/6}}\omega^{-1/2} \quad (5)$$

From the mass balance of each step, the following expressions for k_1, k_2 and k_3 have been derived [4]:

$$k_1 = 0.62D_{O_2}^{2/3}\nu^{-1/6}S_2(I_1 - 1)/(I_1 + 1) \quad (6a)$$

$$k_2 = 0.62D_{O_2}^{2/3}\nu^{-1/6}2S_2/(I_1 + 1) \quad (6b)$$

$$k_3 = 0.62D_{H_2O_2}^{2/3}\nu^{-1/6}NS_1/(I_1N + 1) \quad (6c)$$

where I_1 and S_1 are the intercept and the slope of the I_D/I_R against $\omega^{-1/2}$ plot, respectively, and S_2 is the slope of the $I_{LD}/(I_{LD} - I_D)$ against $\omega^{-1/2}$ plot.

RRDE data for OERR in 0.1 M KOH on different Pt electrodes were plotted as I_D/I_R against $\omega^{-1/2}$ (Fig. 8). These experimental results fulfil Equation 4 in the 0.50 to 0.80 V range. Hence, in principle, the validity of Scheme 3 for the OERR in this potential range is confirmed for platinum in base solution. Thus, as the cathodic overpotential is increased, both the I_D/I_R ratio and the slope of the linear plots become higher. Besides, the linear I_D/I_R against $\omega^{-1/2}$ relationship found for OERR in 0.1 M KOH on A-type platinum becomes ω-independent at potentials lower than 0.60 V. These results reveal that Scheme 3 in
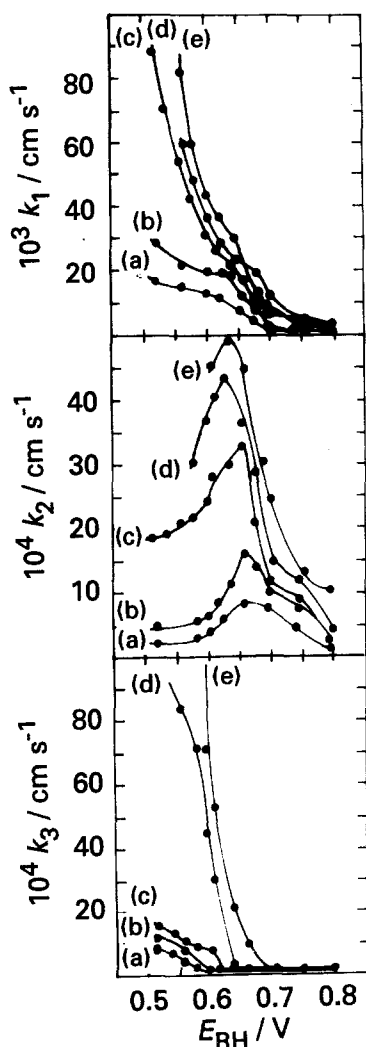
Fig. 10. Plot of k_1, k_2 and k_3 against electrode potentials on polycrystalline Pt in oxygen-saturated KOH solutions: (a) 0.05, (b) 0.1, (c) 0.5, (d) 1 and (e) 3 M.

Fig. 11. Plot of k_1, k_2 and k_3 against electrode potentials on A-type Pt in oxygen-saturated KOH solutions: (a) 0.05, (b) 0.1, (c) 0.5, (d) 1 and (e) 3 M.

the h.c.d. range cannot be straightforwardly applied unless new mechanistic features are included.

The $I_{LD}/(I_{LD} - I_D)$ against $\omega^{-1/2}$ plots for the different platinum working electrode surfaces in 0.1 M KOH are illustrated in Fig. 9. These plots show the same intercept at $I_{LD}/(I_{LD} - I_D) = 1$ for all electrodes, and an increase in the slope of the straight lines as the cathodic overpotential is increased. This behaviour is consistent with data shown in Fig. 5, involving the potential-dependent diffusion correction of OERR polarization curves.

The rate constants k_1, k_2 and k_3 calculated for the different platinum working electrode in KOH solutions are plotted against E_D. For A-type platinum, the value of k_1 increases smoothly on diminishing the potential, and this effect becomes more pronounced when the potential is lower than 0.75 V (Fig. 10). Otherwise, k_2 goes through a maximum value at approximately 0.75 V as it results from the I_R against E_D plot (Fig. 3). The value of k_3, the rate constant of H_2O_2 reduction becomes practically zero over a rather wide potential range for A-type platinum. This potential range becomes narrower as the KOH concentration is increased. Nevertheless, it gives $k_3 = 0$ down to 0.60 V or to 0.68 V depending
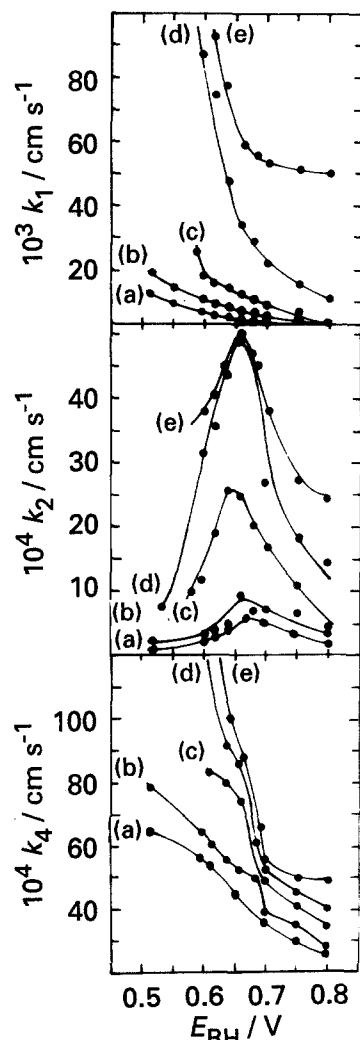
on whether aqueous 0.1 M KOH or 3 M KOH data is considered. This difference is probably due to the fact that the rate of H_2O_2 formation is diminished in 3.0 M KOH because of greater OH^- ion adsorption on platinum. It should be noted that the result $k_3 = 0$ was also reported by Wroblowa *et al.* [32] for the OERR on steel in 1 M NaOH in the 0.80–0.50 V range, and by Bockris *et al.* [33] for the same reaction on passive iron in neutral solutions.

The values of k_1, k_2 and k_3 tend to increase as the KOH concentration is raised on both polycrystalline and B-type platinum (Figs 11 and 12) although their potential dependencies are somewhat similar to that found on A-type platinum. However, in contrast to A-type platinum a finite value of k_3 is always found on polycrystalline and B-type platinum. Besides, k_2 for B-type platinum is almost one order of magnitude lower than those obtained on the other platinum surfaces.

5.3. *Possible structural explanation of adsorbed intermediates at platinum surfaces*

As described earlier [34], scanning tunneling microscopy (STM) imaging of preferred oriented platinum
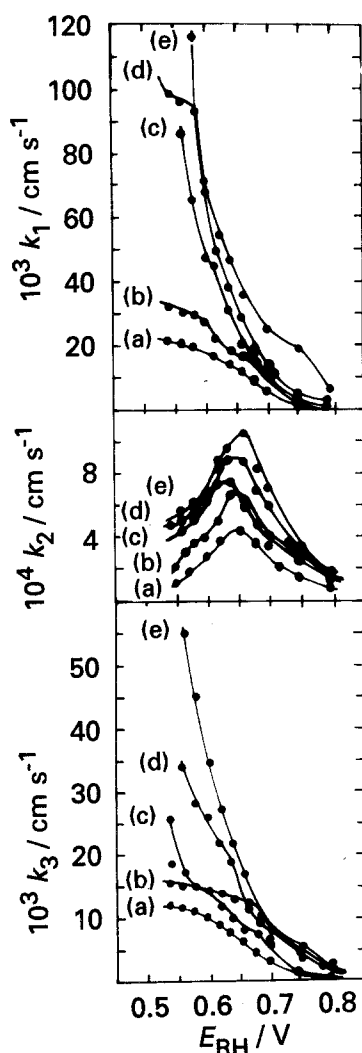
Fig. 12. Plot of k_1, k_2 and k_3 against electrode potentials on B-type Pt in oxygen-saturated KOH solutions: (a) 0.05, (b) 0.1, (c) 0.5, (d) 1 and (e) 3 M.

surfaces show well-defined orientations and a surface topography smoother than that of an untreated poly-crystalline platinum.

The STM images of A-type platinum surfaces show very clear domains of crystallographic orientations comparable to the topography of a Pt(1 0 0) bulk single crystal [35]. The STM images of B-type platinum show a surface structure which is more complex than that of A-type platinum, as it consists of domains with crystallographic features compatible with the (1 1 1) trigonal symmetry, and some others of triangular and three-dimensional polyhedric crystallites [35]. This STM topography of A-type and B-type platinum surfaces reflects on the nanometre scale those seen through the corresponding SEM micrographs on the μm scale [36].

From STM images and voltammetric features of A-type and B-type platinum electrodes it may be concluded that these platinum surfaces can be described as stepped surfaces of high order Miller indices, which are dominated by either (1 0 0) or (1 1 1) crystallographic facets, depending on whether A-type or B-type electrodes are considered. It should be noted that higher order Miller indices surfaces

can be described as combinations of low order Miller indices single crystal faces [37].

The preceding platinum electrode surface description allows us to consider the possible equilibrium structures involved in the interaction of platinum surfaces and reaction intermediates as concluded from the discussion of the OERR kinetics and mechanism already dealt with in Section 4.3., taking into account ideal Pt(1 0 0) and Pt(1 1 1) surfaces, which correspond to the lowest and the highest platinum surface atom density, respectively, as limiting situations. In this way, a tentative explanation about the influence of platinum crystallographic orientation on the OERR kinetics and mechanism can be advanced. The distance between the nearest neighboured platinum atoms, d, is 0.226 nm for Pt(1 1 1) face, 0.277 nm for Pt(1 1 0) face and 0.392 nm for Pt(1 0 0) face [37]. The increase in energy associated with a larger surface area of a metal arises from the fact that surface atoms have fewer neighbours than bulk atoms, contributing less to the total binding energy of the crystal. Accordingly, the relative surface energy varies with the crystalline orientation and the most densely packed structure, namely the Pt(1 1 1) face, should have the greatest surface energy as experimentally demonstrated by Hamelin et al. for gold single crystals in 10 mM NaF [38].

The stability of adsorbed water on single crystal Pt(1 0 0) and Pt(1 1 1) faces was calculated through the extended Hückel theory (EHT). The difference in equilibrium energy values is revealed through the activation energy for H_2O molecule decomposition, which for Pt(1 0 0) is smaller than for Pt(1 1 1). As a first approach, these results can be used to justify the different reactivity of these substrates towards the OERR [39].

The O-containing species bound to platinum involve d-orbitals of the substrate and p-orbitals of oxygen with backdonation to Π^* antibonding orbitals at twofold and fourfold sites depending on the crystalline metal orientation. The adsorption characteristics of oxygen gas on various platinum single crystal faces have been thoroughly investigated [40–45]. Molecularly adsorbed oxygen was found on both polycrystalline platinum [40] and low index platinum faces [40–42]. From vibrational spectroscopical data and near-edge X-ray absorption fine-structure studies (NEXAFS) [45] it is known that molecular oxygen on Pt(1 1 1) forms peroxo-like species at 'on top' sites with an O–O length bond of 0.137 nm, similar to that in aqueous H_2O_2 (0.144 nm) [46]. Furthermore, on Pt(1 1 1) atomic oxygen was also detected above 200 K occupying threefold sites in an ordered p (2 × 2) pattern [41, 44]. Almost the same O–O length bond and LEED patterns were found on Pt(1 1 0) (1 × 2) [47]. Otherwise, oxygen adsorbs molecularly on Pt(1 0 0) (5 × 20) without any dissociation process at temperatures below 123 K [43, 48]. The electronic structure of a p (1 × 1) overlayer on Pt(1 0 0) (1 × 1) was studied by a self-consistent calculation, suggesting that the strongest binding

occurs between adsorbate p-orbitals and platinum d_{xz}, d_{yz} and $d_{x^2-y^2}$-orbitals at fourfold hollow sites [49].

RRDE data obtained at different KOH concentrations showed that the higher amount of H_2O_2 was found at A-type platinum electrodes. So, differences in the OERR mechanism could result from different contributions of the peroxide path to the overall reaction process.

In principle, on the basis of RRDE and gas phase oxygen-adsorption data on platinum single crystals, the relative extent of each OERR parallel reaction pathway at the different platinum surfaces appears to be dependent on the dominating crystallographic structure. Thus, peroxide species are probably more easily produced on A-type platinum, because oxygen is preferentially adsorbed on Pt(1 0 0) crystal faces, which are the dominant faces on A-type platinum. Conversely, O-adsorption seems to be favoured on B-type platinum, which involves a high surface concentration of Pt(1 1 1) sites and correspondingly a smaller amount of H_2O_2 can be produced on this type of platinum electrode.

6. Conclusion

(i) Two different types of OERR behaviour were found depending on the type of facetted platinum electrodes in alkaline solution.

(ii) The amount of H_2O_2 found for A-type platinum was higher than that for the other platinum surfaces in all KOH solutions.

(iii) The presence of H_2O_2 or SO_4^{2-} ion in KOH solution produces a blockage of the electrode surface leading to higher Tafel slopes and lower cathodic currents in h.c.d. region.

(iv) An increase in KOH concentration produces a lower amount of H_2O_2 at all platinum surfaces, due to a competitive adsorption between oxygen and OH^- ion from the electrolyte.

(v) OERR on polycrystalline and B-type platinum proceeds through a direct four-electron pathway to OH^- ion with peroxide species as intermediates.

(vi) A complete reduction from oxygen to OH^- takes place on A-type platinum, in parallel with a two-electron process in which H_2O_2 is produced.

Acknowledgements

References

[1] S. Srinivasan and J. O'M. Bockris, 'Fuel Cells: Their Electrochemistry', McGraw-Hill, New York (1969) Chapter 9.

[2] M. W. Breiter, 'Electrochemical Processes in Fuel Cells', Springer-Verlag, New York (1969).

[3] M. R. Tarasevich, A. Sadkowski and E. B. Yeager, in 'Comprehensive Treatise of Electrochemistry' (edited by J. O'M. Bockris, E. B. Yeager, S. U. M. Kahn and R. E. White), Vol. 7, Plenum Press, New York (1983) Chapter 7, p. 301.

[4] E. Yeager, Electrochim. Acta 29 (1984) 1527.

[5] Su-Moon Park, S. Ho, S. Aruliah, M. Weber, C. Ward, R. Venter and S. Srinivasan, J. Electrochem. Soc. 113 (1986) 1641.

[6] A. Damjanovic, M. Genshaw and J. O'M. Bockris, ibid. 114 (1967) 1107.

[7] D. Sepa, E. M. Vojnovic and A. Damjanovic, Electrochim. Acta 25 (1979) 149.

[8] F. El Kadiri, R. Faure and R. Durand, J. Electroanal. Chem. 301 (1991) 177.

[9] C. F. Zinola, A. M. Castro Luna, W. E. Triaca and A. J. Arvia, to be published.

[10] W. E. O'Grady, E. J. Taylor and S. Srinivasan, J. Electroanal. Chem. 1132 (1992) 1147.

[11] A. E. Bolzán, A. M. Castro Luna, A. Visintín, R. C. Salvarezza and A. J. Arvia, Electrochim. Acta 33 (1988) 1743.

[12] W. J. Albery and S. Brückenstein, Trans. Faraday Soc. 62 (1966) 1920.

[13] H. Angerstein-Kozlowska, in 'Comprehensive Treatise of Electrochemistry', (edited by E. B. Yeager, J. O'M. Bockris, B. E. Conway and S. Sarangapani), Vol. 9, Plenum Press, New York/London (1984) Chapter 2, pp. 15–61.

[14] A. Visintín, W. E. Triaca and A. J. Arvia, J. Electroanal. Chem. 284 (1990) 465.

[15] K. Dj. Popovic, N. M. Markovic, A. V. Tripkovic and R. R. Adzic, ibid. 313 (1991) 184.

[16] K. E. Gubbin and R. D. Walker, J. Electrochem. Soc. 112 (1965) 469.

[17] H. S. Harned and M. A. Cook, J. Am. Chem. Soc. 59 (1937) 496.

[18] M. K. Tham, R. D. Walker and K. E. Gubbin, J. Phys. Chem. 74 (1970) 1747.

[19] 'International Critical Tables', Vol. VII, 4th edn, (edited by E. W. Washburn), McGraw-Hill, New York (1933) p. 212.

[20] K. A. Striebel, F. R. McLarnon and E. J. Cairns, J. Electrochem. Soc. 137 (1990) 3351.

[21] V. G. Levich, 'Physicochemical Hydrodynamics', Prentice Hall, Englewood Cliffs, NJ (1962).

[22] F. C. Nart and T. Iwasita, J. Electroanal. Chem. 308 (1991) 277.

[23] E. Gileadi, S. Argade and J. O'M. Bockris, J. Phys. Chem. 70 (1966) 2044.

[24] J. C. Huang, R. K. Sen and E. Yeager, J. Electrochem. Soc. 126 (1979) 786.

[25] A. Damjanovic, M. A. Genshaw and J. O'M. Bockris, J. Chem. Phys. 45 (1964) 4057.

[26] R. W. Zurilla, R. K. Sen and E. B. Yeager, J. Electrochem. Soc. 125 (1978) 1123.

[27] H. S. Wroblowa, Y. C. Pan and G. Razumney, J. Electroanal. Chem. 69 (1976) 195.

[28] L. Müller and L. N. Nekrasov, Electrochim. Acta 9 (1964) 1015.

[29] M. R. Tarasevich, Elektrokhimiya 4 (1968) 210.

[30] A. J. Appleby and M. V. Savy, J. Electroanal. Chem. 92 (1978) 15.

[31] K. L. Hsueh, E. R. González, S. Srinivasan and D. T. Chin, J. Electrochem. Soc. 131 (1984) 823.

[32] H. S. Wroblowa and S. B. Qaderi, J. Electroanal. Chem. 279 (1990) 231.

[33] V. Jovancicevic and J. O'M. Bockris, J. Electrochem. Soc. 133 (1986) 1797.

[34] L. Vázquez, J. M. Gómez Rodríguez, J. Gómez Herrero, A. M. Baró, N. García, J. C. Canullo and A. J. Arvia, Surf. Sci. 181 (1987) 98.

[35] J. Gómez, L. Vázquez, A. M. Baró, N. García, C. L. Perdriel, W. E. Triaca and A. J. Arvia, Nature 323 (1986) 612.

[36] R. M. Cerviño, A. J. Arvia and W. E. Vielstich, Surf. Sci. 154 (1985) 623.

[37] A. Hamelin, in 'Modern Aspects of Electrochemistry', (edited by B. E. Conway, J. O'M. Bockris and R. E.

White), Vol. 16, Plenum Press, New York (1985) Chapter 1.

[38] A. Hamelin, T. Vitanov, E. Sevastianov and A. Popov, *J. Electroanal. Chem.* **145** (1985) 225.

[39] G. Estiú, S. A. Maluendes, E. A. Castro and A. J. Arvia, *J. Phys. Chem.* **92** (1988) 2512.

[40] P. R. Norton, *Surf. Sci.* **47** (1975) 98.

[41] H. Steininger, S. Lehwald and H. Ibach, *Surf. Sci.* **123** (1982) 1.

[42] C. T. Campbell, G. Ertl, H. Kuipers and J. Segner, *Surf. Sci.* **107** (1981) 220.

[43] M. A. Barteau, E. I. Ko and R. J. Madix, *ibid.* **102** (1981) 99.

[44] J. L. Gland, B. A. Sexton and G. B. Fisher, *ibid.* **95** (1980) 587.

[45] G. Maure, P. Légaré and G. Lindauer, *ibid.* **80** (1979) 238.

[46] J. Stöhr, J. L. Gland, W. Eberhardt, D. Outka, R. J. Madix, F. Sette, R. J. Koestner and U. Doebler, *Phys. Rev. Lett.* **51** (1983) 2414.

[47] Y. Ohno, T. Matsushima, S. Tanaka, E. Yagasaki and M. Kamada, *Surf. Sci.* **275** (1992) 281.

[48] P. R. Norton, P. E. Binder and K. Griffiths, *J. Vac. Sci. Technol.* **A2** (1984) 1028.

[49] G. A. Benesh and L. S. G. Liyanage, *Surf. Sci.* **261** (1992) 207.